A symmetric integrated radial basis function method for solving differential equations

N. Mai-Duy*, D. Dalal, T.T.V. Le, D. Ngo-Cong and T. Tran-Cong
Computational Engineering and Science Research Centre,
School of Mechanical and Electrical Engineering,
University of Southern Queensland, Toowoomba, QLD 4350, Australia

Submitted to *Numerical Methods for Partial Differential Equations*,
March/2017; revised, November/2017

Abstract In this paper, integrated radial basis functions (IRBFs) are employed for Hermite interpolation in the solution of differential equations, resulting in a new meshless symmetric RBF method. Both global and local approximation-based schemes are derived. For the latter, the focus is on the construction of compact approximation stencils, where a sparse system matrix and a high-order accuracy can be achieved together. Cartesian-grid-based stencils are possible for problems defined on non-rectangular domains. Furthermore, the effects of the RBF width on the solution accuracy for a given grid size are fully explored with a reasonable computational cost. The proposed schemes are numerically verified in some elliptic boundary-value problems governed by the Poisson and convection-diffusion equations. High levels of the solution accuracy are obtained using relatively coarse discretisations.

Keywords: Hermite interpolation, global approximation, compact local approximation, integrated radial basis function, flat radial basis function, extended precision

*Corresponding author E-mail: nam.mai-duy@usq.edu.au, Telephone +61-7-46312748, Fax +61-7-46312529

1 Introduction

Radial basis function (RBF) methods have become a powerful means of representing functions and solving ordinary/partial differential equations (ODEs/PDEs). For strict interpolation (noiseless data), a target function can be represented by a linear combination of RBFs. According to Micchelli's theorem [1], for a large class of RBFs, their interpolation matrices constructed from the distinct data points are guaranteed to be invertible. Examples of RBFs that are covered by Micchelli's theorem and of particular interest in practice are the multiquadric, inverse multiquadric and Gaussian functions. Unlike conventional interpolation schemes, the quality of approximations based on these infinitely smooth RBFs can be controlled not only by the number of data points (i.e. the number of RBFs) but also by the RBF widths (also called the free/shape parameters). Furthermore, RBF methods are capable of yielding spectral accuracy with respect to the number of RBFs and/or their widths [2]. Application of RBFs to the numerical solution of PDEs was proposed by Kansa in 1990 [3]. In Kansa's method, the PDE is discretised by means of point collocation and a field variable is approximated by a set of multiquadric functions with a differentiation process being employed to obtain basis functions for derivative terms in the PDE (DRBFs). Since then, the RBF solution to differential problems has received a great deal of attention (see, e.g., [4-14]). For a given node distribution, the solution accuracy can still be improved by changing the value of the RBF width. Finding the optimal RBF width for a general case still presents a great challenge. In practice, one may rely on numerical algorithms such as those based on statistics (cross validation and maximum likelihood estimation) for determining this value. For a smooth function, the best accuracy can often be achieved at a large RBF width (i.e. near-flat RBF). As the RBF width increases, its matrix condition number grows rapidly and one needs stable-calculation algorithms for obtaining a reliable numerical solution (see, e.g., [15-20]). The issue of stagnation errors (i.e. failure of convergence under continuing node refinement) was recently discussed in [21] along with several treatments proposed to overcome it. It should be noted that the system matrix resulting from Kansa's method may not be invertible for certain configurations of RBF centres and certain kinds of differential operators as numerically demonstrated in [22].

For data containing both function and derivative values, one can employ the RBF Hermite interpolation approach [23-25]. Its applications in the solution of ODEs/PDEs were reported in, e.g., [26-28]. The main advantage of this approach is that it can yield an interpolation matrix that is symmetric and invertible for both function representation and solution of ODEs/PDEs. The symmetric property also allows for the saving of computer storage space and the use of a more efficient algebraic solver. In addition, the RBF Hermite interpolation approach was also utilised to construct compact local approximations (see, e.g., [29,16,30]). This kind of application has attracted more attention in recent years as both a sparse system matrix and a fast convergence rate of the solution can be achieved together.

Integrated RBFs (IRBFs) have been proposed for solving ODEs/PDEs (see, e.g., [31-35,4]). In IRBF methods, basis functions used for the approximation of a field variable are obtained by integrating RBFs. Numerical experiments showed that IRBF methods can yield an improved rate of convergence. In previous reports [30,36,37], we integrated RBFs with respect to the Cartesian coordinates (i.e. x, y and z). Through integration constants, nodal derivative values can be incorporated into the IRBF expressions. Their associated basis functions are generally not radial and the resultant IRBF matrices are nonsymmetric. In this work, RBFs are integrated with respect to the radius without the addition of integration constants. All derived basis functions are radial and they are employed for Hermite interpolation. Both global and local approximations are considered, producing new strong forms of the IRBF approach. For the former, the interpolation at a point involves function values at all nodes and therefore its system matrix is fully populated. For the latter, compact IRBF approximations are constructed on small stencils, resulting in a sparse system matrix. For both versions, the interpolation matrix is symmetric. The obtained IRBF results are compared with those by the classical finite-difference methods (FDMs), compact FDMs, and Hermite methods based on differentiated RBFs. The rest of the paper is organised as follows. In Section 2, relevant basis functions for DRBFs and IRBFs are provided. Global and local schemes of the proposed IRBF Hermite-based method are presented and verified in Sections 3 and 4, respectively. Section 5 gives some concluding remarks. In Appendix, the process of acquiring the limit of the fourth-order cross derivative as the radius approaches zero is described.

2 Basis functions for DRBFs and IRBFs

For DRBFs, a function can be represented by a linear combination of RBFs

$$f(\mathbf{x}) = \sum_{j=1}^{N} w_j \varphi(\|\mathbf{x} - \mathbf{x}_j\|), \tag{1}$$

where N is the number of given data points, $\{\varphi(r = \|\mathbf{x} - \mathbf{x}_j\|)\}_{j=1}^{N}$ a set of RBFs, $\{\mathbf{x}_j\}_{j=1}^{N}$ a set of centres which is normally chosen to be the same as a set of data points, and $\{w_j\}_{j=1}^{N}$ a set of weights to be found. It has been theoretically shown that the interpolation matrix derived from (1) on a set of distinct points is nonsingular if φ is a positive definite function such as the inverse multiquadric and Gaussian functions, or a conditionally positive definite function of order 1 such as the multiquadric function [1]. In this work, RBF is taken as the multiquadric (MQ) function

$$\varphi(r) = \sqrt{r^2 + a^2}, \tag{2}$$

where a is the MQ width.

Derivatives of function f can then be determined as, e.g., in two dimensions

$$\frac{\partial^k f(\mathbf{x})}{\partial x^k} = \sum_{j=1}^{N} w_j \frac{\partial^k \varphi(\|\mathbf{x} - \mathbf{x}_j\|)}{\partial x^k}, \quad k = 1, 2, 3, \cdots, \tag{3}$$

$$\frac{\partial^k f(\mathbf{x})}{\partial y^k} = \sum_{j=1}^{N} w_j \frac{\partial^k \varphi(\|\mathbf{x} - \mathbf{x}_j\|)}{\partial y^k}, \quad k = 1, 2, 3, \cdots, \tag{4}$$

$$\frac{\partial^k f(\mathbf{x})}{\partial x^m \partial y^n} = \sum_{j=1}^{N} w_j \frac{\partial^k \varphi(\|\mathbf{x} - \mathbf{x}_j\|)}{\partial x^m \partial y^n}, \quad m = 1, 2, \cdots,\ n = 1, 2, \cdots,\ k = m + n. \tag{5}$$

Expressions for computing derivatives of (2) with respect to r up to the fourth order are

$$\frac{d\varphi}{dr} = \frac{r}{\sqrt{r^2 + a^2}}, \tag{6}$$

$$\frac{d^2\varphi}{dr^2} = \frac{a^2}{(r^2 + a^2)^{3/2}}, \tag{7}$$

$$\frac{d^3\varphi}{dr^3} = -\frac{3a^2 r}{(r^2 + a^2)^{5/2}}, \tag{8}$$

$$\frac{d^4\varphi}{dr^4} = -\frac{3a^2 (a^2 - 4r^2)}{(r^2 + a^2)^{7/2}}. \tag{9}$$

For IRBFs, a function is decomposed into a set of basis functions that are obtained from integrating (2) with respect to r. Below is the case, where the MQ is integrated 4 times

$$\bar{\varphi}(r) = \left(\frac{a^4}{45} - \frac{83a^2r^2}{720} + \frac{r^4}{120}\right)\sqrt{r^2+a^2} + \left(-\frac{a^4 r}{16} + \frac{a^2 r^3}{12}\right)\ln\left(\frac{r+\sqrt{r^2+a^2}}{a}\right), \tag{10}$$

$$\begin{aligned}
\frac{d\bar{\varphi}}{dr} &= \left(-\frac{13a^2r}{48} + \frac{r^3}{24}\right)\sqrt{r^2+a^2} + \left(-\frac{a^4}{16} + \frac{a^2r^2}{4}\right)\ln\left(\frac{r+\sqrt{r^2+a^2}}{a}\right), && (11)\\
\frac{d^2\bar{\varphi}}{dr^2} &= \left(-\frac{a^2}{3} + \frac{r^2}{6}\right)\sqrt{r^2+a^2} + \frac{a^2 r}{2}\ln\left(\frac{r+\sqrt{r^2+a^2}}{a}\right), && (12)\\
\frac{d^3\bar{\varphi}}{dr^3} &= \frac{r}{2}\sqrt{r^2+a^2} + \frac{a^2}{2}\ln\left(\frac{r+\sqrt{r^2+a^2}}{a}\right), && (13)\\
\frac{d^4\bar{\varphi}}{dr^4} &= \sqrt{r^2+a^2}. && (14)
\end{aligned}$$

Figure 1 illustrates the shape of the MQ (2) and the integrated MQ (10) for several values of the MQ width. It was shown in [33] that the integrated MQ approaches a large constant as $1/a$ approaches zero. Both DRBFs and IRBFs are implemented in this work. For simplicity of notation, expression (1) is now used for the two approaches, where function $\varphi(r)$ is taken in the form of (2) for DRBFs and in the form of (10) for IRBFs. We introduce the concept of order for IRBF. An IRBF is said to be of order α if its (original) RBF is integrated α times. For function φ defined in (10), one has $\alpha = 4$. As shown in [33], this IRBF is a conditionally positive definite function of order $(\alpha+2)/2 = 3$ and from a theoretical point of view, one needs to add to the interpolant a polynomial whose order is less by 1 (i.e. 2) to acquire an invertible interpolation matrix. However, from numerical experiments reported, to our best knowledge, a singular interpolation matrix was never observed when the IRBF approximations were not augmented with polynomial terms. Furthermore, the addition of a polynomial did not lead to any significant improvement in the solution accuracy at relatively coarse disretisations.

An effective way to compute derivatives of function φ with respect to x and y on RHS of (3)-(5) ($k = \{1,2,3,4\}$, $m = n = 2$) is to express them in terms of derivatives of φ with respect to r. Since their expressions in the x and y coordinates are of similar forms, only

pure derivatives with respect to x together with cross derivatives are given below

$$\frac{\partial \varphi}{\partial x} = \frac{d\varphi}{dr}\frac{\partial r}{\partial x}, \tag{15}$$

$$\frac{\partial^2 \varphi}{\partial x^2} = \frac{d\varphi}{dr}\frac{\partial^2 r}{\partial x^2} + \frac{d^2\varphi}{dr^2}\left(\frac{\partial r}{\partial x}\right)^2, \tag{16}$$

$$\frac{\partial^3 \varphi}{\partial x^3} = \frac{d\varphi}{dr}\frac{\partial^3 r}{\partial x^3} + 3\frac{d^2\varphi}{dr^2}\frac{\partial r}{\partial x}\frac{\partial^2 r}{\partial x^2} + \frac{d^3\varphi}{dr^3}\left(\frac{\partial r}{\partial x}\right)^3, \tag{17}$$

$$\frac{\partial^4 \varphi}{\partial x^4} = \frac{d\varphi}{dr}\frac{\partial^4 r}{\partial x^4} + \frac{d^2\varphi}{dr^2}\left[4\frac{\partial r}{\partial x}\frac{\partial^3 r}{\partial x^3} + 3\left(\frac{\partial^2 r}{\partial x^2}\right)^2\right] + 6\frac{d^3\varphi}{dr^3}\left(\frac{\partial r}{\partial x}\right)^2\frac{\partial^2 r}{\partial x^2} + \frac{d^4\varphi}{dr^4}\left(\frac{\partial r}{\partial x}\right)^4, \tag{18}$$

$$\frac{\partial^4 \varphi}{\partial x^2 \partial y^2} = \frac{d\varphi}{dr}\frac{\partial^4 r}{\partial x^2 \partial y^2} + \frac{d^2\varphi}{dr^2}\left[\frac{\partial^2 r}{\partial x^2}\frac{\partial^2 r}{\partial y^2} + 2\left(\frac{\partial^2 r}{\partial x \partial y}\right)^2 + 2\frac{\partial r}{\partial x}\frac{\partial^3 r}{\partial x \partial y^2} + 2\frac{\partial r}{\partial y}\frac{\partial^3 r}{\partial x^2 \partial y}\right] + \frac{d^3\varphi}{dr^3}\left[\frac{\partial^2 r}{\partial y^2}\left(\frac{\partial r}{\partial x}\right)^2 + 4\frac{\partial r}{\partial x}\frac{\partial r}{\partial y}\frac{\partial^2 r}{\partial x \partial y} + \frac{\partial^2 r}{\partial x^2}\left(\frac{\partial r}{\partial y}\right)^2\right] + \frac{d^4\varphi}{dr^4}\left(\frac{\partial r}{\partial x}\right)^2\left(\frac{\partial r}{\partial y}\right)^2. \tag{19}$$

Since

$$r = \|\mathbf{x} - \mathbf{x}_j\| = \sqrt{(x - x_j)^2 + (y - y_j)^2}, \tag{20}$$

expressions for computing pure and cross derivatives of r on RHS of (15)-(19) are given by

$$\frac{\partial r}{\partial x} = \frac{x - x_j}{r}, \tag{21}$$

$$\frac{\partial^2 r}{\partial x^2} = \frac{r^2 - (x - x_j)^2}{r^3}, \tag{22}$$

$$\frac{\partial^3 r}{\partial x^3} = -\frac{3(x - x_j)\left[r^2 - (x - x_j)^2\right]}{r^5}, \tag{23}$$

$$\frac{\partial^4 r}{\partial x^4} = -\frac{3\left[r^2 - (x - x_j)^2\right]\left[r^2 - 5(x - x_j)^2\right]}{r^7}, \tag{24}$$

$$\frac{\partial^2 r}{\partial x \partial y} = -\frac{(x - x_j)(y - y_j)}{r^3}, \tag{25}$$

$$\frac{\partial^3 r}{\partial x \partial y^2} = \frac{(x - x_j)\left[-(x - x_j)^2 + 2(y - y_j)^2\right]}{r^5}, \tag{26}$$

$$\frac{\partial^3 r}{\partial x^2 \partial y} = \frac{(y - y_j)\left[-(y - y_j)^2 + 2(x - x_j)^2\right]}{r^5}, \tag{27}$$

$$\frac{\partial^4 r}{\partial x^2 \partial y^2} = \frac{2}{r^3} - \frac{15(x - x_j)^2(y - y_j)^2}{r^7}. \tag{28}$$

The limits of derivatives of function φ when $r \to 0$ are

$$\frac{\partial \varphi}{\partial x} \to 0, \quad \frac{\partial^2 \varphi}{\partial x^2} \to \frac{1}{a}, \quad \frac{\partial^3 \varphi}{\partial x^3} \to 0, \quad \frac{\partial^4 \varphi}{\partial x^4} \to -\frac{3}{a^3}, \tag{29}$$

$$\frac{\partial \varphi}{\partial y} \to 0, \quad \frac{\partial^2 \varphi}{\partial y^2} \to \frac{1}{a}, \quad \frac{\partial^3 \varphi}{\partial y^3} \to 0, \quad \frac{\partial^4 \varphi}{\partial y^4} \to -\frac{3}{a^3}, \tag{30}$$

$$\frac{\partial^4 \varphi}{\partial x^2 \partial y^2} \to -\frac{1}{a^3}, \tag{31}$$

for DRBF and

$$\frac{\partial \varphi}{\partial x} \to 0, \quad \frac{\partial^2 \varphi}{\partial x^2} \to -\frac{a^3}{3}, \quad \frac{\partial^3 \varphi}{\partial x^3} \to 0, \quad \frac{\partial^4 \varphi}{\partial x^4} \to a, \tag{32}$$

$$\frac{\partial \varphi}{\partial y} \to 0, \quad \frac{\partial^2 \varphi}{\partial y^2} \to -\frac{a^3}{3}, \quad \frac{\partial^3 \varphi}{\partial y^3} \to 0, \quad \frac{\partial^4 \varphi}{\partial y^4} \to a, \tag{33}$$

$$\frac{\partial^4 \varphi}{\partial x^2 \partial y^2} \to \frac{a}{3}, \tag{34}$$

for IRBF. It is straightforward to obtain results (29), (30), (32) and (33). For (31) and (34), one may need to replace the biharmonic operator with Laplace ones, and the detailed process is described in Appendix.

As discussed early, the quality of approximations by the MQs is dependent on both their spacing and width. For an easy interpretation, the MQ width a is expressed in terms of a typical distance from the MQ centre to its neighbours, denoted by h, as

$$a = \beta h, \tag{35}$$

where β is a constant that can run from a small to large positive value. For a given node distribution, the value of h can be determined. The advantage of (35) lies in its simplicity with β being a dimensionless quantity.

For the node refinement (scheme resolution), the value of h is reduced. In practice, the RBF width is then chosen to be smaller by, for example, keeping β fixed. It was shown in [21], this common practice may lead to the issue of stagnation errors (i.e. failure of convergence in the $h \to 0$ limit), which can be overcome by adding polynomial terms to the interpolant or keeping the RBF width fixed (i.e. fixed a). On the other hand, for a given grid size (fixed

h), one can change β to improve the RBF approximations. In this case, it is expected that the addition of polynomial terms will not affect much the solution accuracy.

In this study, we focus on investigating the effects of β on the solution accuracy for a given grid size. A wide range of β is explored by using the extended precision approach. Grid refinements are also studied; however, only relatively coarse grids are considered, for which the formula (35) can be applied without causing stagnation errors. It will be shown later that the simple formula (35) can produce results that are very close to the ones corresponding to the best values of β over a range of grid sizes.

Numerical experiments indicate that IRBFs lead to matrices of higher condition numbers than DRBFs. For a smooth function, accurate approximations by the former may thus occur earlier as β increases. In this regard, the comparison of accuracy between DRBFs and IRBFs should be made over a wide range of β rather than at its some particular values. For the presented numerical examples, in comparing the two RBF methods, a range of β is considered as wide as possible.

3 IRBF Hermite-based method: global scheme

Consider a differential problem

$$\mathcal{L}u(\mathbf{x}) = b(\mathbf{x}), \quad \mathbf{x} \in \Omega, \tag{36}$$

$$\mathcal{B}u(\mathbf{x}) = s(\mathbf{x}), \quad \mathbf{x} \in \Gamma, \tag{37}$$

where Ω and Γ are a bounded domain and its boundary, $\mathcal{L}$ and $\mathcal{B}$ some linear differential operators, and b and s given functions. Let N be the total number of nodes and N_b the number of boundary nodes ($N_b < N$). The field variable is approximated as

$$u(\mathbf{x}) = \sum_{j=1}^{N_b} w_j \mathcal{B}^{\mathbf{x}_j} \varphi(\|\mathbf{x} - \mathbf{x}_j\|) + \sum_{j=N_b+1}^{N} w_j \mathcal{L}^{\mathbf{x}_j} \varphi(\|\mathbf{x} - \mathbf{x}_j\|) + \sum_{k=1}^{M} v_k p_k(\mathbf{x}), \tag{38}$$

where φ is given by (10) for IRBFs and (2) for DRBFs, the notations $\mathcal{L}^{\mathbf{x}_j}$ and $\mathcal{B}^{\mathbf{x}_j}$ mean that $\mathcal{L}$ and $\mathcal{B}$ act on φ considered as a function of the variable $\mathbf{x}_j$, and $\{p_k(\mathbf{x})\}_{k=1}^{M}$ is a basis for the M-dimensional space ($\prod_m^d$) of all d-variate polynomials that have degree less than or equal to m. The degree of the additional polynomial in (38) is dependent on the form of φ employed, for example, $m = 2$ for (10) and $m = 0$ for (2) as shown in Section 2. To account for the addition of polynomial terms, the following extra constraints are imposed

$$\sum_{j=1}^{N_b} w_j \mathcal{B}^{\mathbf{x}} p_k(\mathbf{x})|_{\mathbf{x}=\mathbf{x}_j} + \sum_{j=N_b+1}^{N} w_j \mathcal{L}^{\mathbf{x}} p_k(\mathbf{x})|_{\mathbf{x}=\mathbf{x}_j} = 0, \quad k = 1, 2, \ldots, M. \tag{39}$$

Substitution of (38) into (37) and (36) yield

$$\sum_{j=1}^{N_b} w_j \mathcal{B}^{\mathbf{x}} \mathcal{B}^{\mathbf{x}_j} \varphi(\|\mathbf{x} - \mathbf{x}_j\|) + \sum_{j=N_b+1}^{N} w_j \mathcal{B}^{\mathbf{x}} \mathcal{L}^{\mathbf{x}_j} \varphi(\|\mathbf{x} - \mathbf{x}_j\|) + \sum_{k=1}^{M} v_k \mathcal{B}^{\mathbf{x}} p_k(\mathbf{x}) = s(\mathbf{x}), \tag{40}$$

$$\sum_{j=1}^{N_b} w_j \mathcal{L}^{\mathbf{x}} \mathcal{B}^{\mathbf{x}_j} \varphi(\|\mathbf{x} - \mathbf{x}_j\|) + \sum_{j=N_b+1}^{N} w_j \mathcal{L}^{\mathbf{x}} \mathcal{L}^{\mathbf{x}_j} \varphi(\|\mathbf{x} - \mathbf{x}_j\|) + \sum_{k=1}^{M} v_k \mathcal{L}^{\mathbf{x}} p_k(\mathbf{x}) = b(\mathbf{x}). \tag{41}$$

Collocation of (40) at the boundary points and of (41) at the interior grid nodes, together with (39), result in a set of $(N + M)$ algebraic equations for $(N + M)$ unknowns, namely $\{w_j\}_{j=1}^{N}$ and $\{v_k\}_{k=1}^{M}$, in which the system matrix is symmetric.

When the augmented polynomial is excluded from the RBF approximations, equations (40), (41) and (39) reduce to

$$\sum_{j=1}^{N_b} w_j \mathcal{B}^{\mathbf{x}} \mathcal{B}^{\mathbf{x}_j} \varphi(\|\mathbf{x} - \mathbf{x}_j\|) + \sum_{j=N_b+1}^{N} w_j \mathcal{B}^{\mathbf{x}} \mathcal{L}^{\mathbf{x}_j} \varphi(\|\mathbf{x} - \mathbf{x}_j\|) = s(\mathbf{x}), \tag{42}$$

$$\sum_{j=1}^{N_b} w_j \mathcal{L}^{\mathbf{x}} \mathcal{B}^{\mathbf{x}_j} \varphi(\|\mathbf{x} - \mathbf{x}_j\|) + \sum_{j=N_b+1}^{N} w_j \mathcal{L}^{\mathbf{x}} \mathcal{L}^{\mathbf{x}_j} \varphi(\|\mathbf{x} - \mathbf{x}_j\|) = b(\mathbf{x}), \tag{43}$$

which lead to a set of only N algebraic equations for N unknowns.

3.1 ODEs

We apply the methods to the following second-order ODE $d^2u/dx^2 = -4\pi^2 \sin(2\pi x), \quad 0 \leq x \leq 1$, subject to Dirichlet boundary conditions. The exact solution can be verified to be $u_e(x) = \sin(2\pi x)$.

Equations (40), (41) and (39) take the form

$$\sum_{j=1}^{2} w_j \varphi(\|x - x_j\|) + \sum_{j=3}^{N} w_j \frac{d^2\varphi(\|x - x_j\|)}{dx_j^2} + \sum_{k=1}^{3} v_k p_k(x) = \sin(2\pi x), \tag{44}$$

$$\sum_{j=1}^{2} w_j \frac{d^2\varphi(\|x - x_j\|)}{dx^2} + \sum_{j=3}^{N} w_j \frac{d^4\varphi(\|x - x_j\|)}{dx^2 dx_j^2} + \sum_{k=1}^{3} v_k \frac{d^2 p_k(x)}{dx^2} = -4\pi^2 \sin(2\pi x), \tag{45}$$

$$\sum_{j=1}^{2} w_j p_k(x_j) + \sum_{j=3}^{N} w_j \frac{d^2 p_k(x_j)}{dx^2} = 0, \quad k = \{1, 2, 3\}. \tag{46}$$

When the RBF approximations are not augmented with the polynomial terms, the above equations become

$$\sum_{j=1}^{2} w_j \varphi(\|x - x_j\|) + \sum_{j=3}^{N} w_j \frac{d^2\varphi(\|x - x_j\|)}{dx_j^2} = \sin(2\pi x), \tag{47}$$

$$\sum_{j=1}^{2} w_j \frac{d^2\varphi(\|x - x_j\|)}{dx^2} + \sum_{j=3}^{N} w_j \frac{d^4\varphi(\|x - x_j\|)}{dx^2 dx_j^2} = -4\pi^2 \sin(2\pi x). \tag{48}$$

We first compare the numerical performance of (44)-(46) and (47)-(48). The problem domain is discretised using a set of uniformly distributed points. We take h in (35) as the grid size. In the global scheme, the RBF approximations involve all nodes and therefore their matrix condition number is expected to grow rapidly. Values of β here should be chosen to be relatively small. The IRBF and DRBF results concerning the relative L_2 error, denoted by N_e, against the RBF width, displayed through β, are depicted in Figure 2, showing that the IRBF/DRBF solutions of the two systems (i.e. (44)-(46) and (47)-(48)) have similar behaviour. However, for IRBFs, the one without the augmented polynomial is slightly more accurate. It appears that adding polynomial terms to the interpolants for the case of a fixed h does not lead an improvement in accuracy. For both cases (i.e. with and without the polynomial terms), we did not experience any singular interpolation matrix over a full range

of the RBF width. These observations are consistent with remarks of other computational works in the RBF literature.

In Figure 3, results by the IRBF and DRBF Hermite-based methods are compared together for a given grid size. It can be seen that the former is generally more accurate than the latter over a wide range of β. As β increases, the computed errors of the two methods fluctuate due to their higher matrix condition numbers. Several algorithms to extend the working range of the RBF width have been proposed in the literature (see, e.g. [15-19,37]). In this work, we employ the extended precision approach. Our programs are written in Matlab with function vpa being utilised to increase the number of significant figures from 16 to 50. As shown in Figure 3, the calculation is now stable over the full range of the RBF width. Results obtained indicate that the use of IRBFs leads to a significantly improved accuracy from a small to large RBF width. The best accuracy by the two methods corresponds to similar values of β.

Figure 4 displays the effects of the grid size on the solution accuracy by the proposed global Hermite-based method for several values of β. The domain is represented by uniform grids, $\{101, 111, \cdots, 1001\}$. A relation between N_e and h in the log-log scale is fitted by a linear function with its slope being regarded as an average rate of convergence. The IRBF solution converges as $O(h^{2.83})$ for $\beta = 1$, $O(h^{2.96})$ for $\beta = 3$ and $O(h^{2.90})$ for $\beta = 5$. Highly accurate results are obtained; the relative L_2 error is reduced to $O(10^{-10})$ for $\beta = 5$. Also, constant values of β produce similar rates of convergence; larger β corresponds to a higher level of accuracy. These simple behaviours provide some useful guidance on how to choose the RBF width in practical applications.

3.2 PDEs

We apply the methods to Poisson equation with its driving function $b = -2\pi^2 \sin(\pi x) \sin(\pi y)$ and $0 \leq x, y \leq 1$. The exact solution can be verified to be $u_e(x, y) = \sin(\pi x) \sin(\pi y)$ from which one can obtain Dirichlet boundary conditions.

For Poisson equation, $\mathcal{L}^{\mathbf{x}}$ and $\mathcal{L}^{\mathbf{x}_j}$ take the form

$$\mathcal{L}^{\mathbf{x}} = \frac{\partial^2}{\partial x^2} + \frac{\partial^2}{\partial y^2}, \tag{49}$$

$$\mathcal{L}^{\mathbf{x}_j} = \frac{\partial^2}{\partial x_j^2} + \frac{\partial^2}{\partial y_j^2}. \tag{50}$$

Since $\mathbf{x}$ and $\mathbf{x}_j$ can be interchanged in defining the input r of MQ, one has

$$\begin{aligned} \mathcal{L}^{\mathbf{x}}\mathcal{L}^{\mathbf{x}_j} &= \left(\frac{\partial^2}{\partial x^2} + \frac{\partial^2}{\partial y^2}\right)\left(\frac{\partial^2}{\partial x_j^2} + \frac{\partial^2}{\partial y_j^2}\right), \\ &= \frac{\partial^4}{\partial x^4} + 2\frac{\partial^4}{\partial x^2 \partial y^2} + \frac{\partial^4}{\partial y^4} = \frac{\partial^4}{\partial x_j^4} + 2\frac{\partial^4}{\partial x_j^2 \partial y_j^2} + \frac{\partial^4}{\partial y_j^4}. \end{aligned} \tag{51}$$

We employ 4 set of unstructured nodes to represent the problem domain (Figure 5). The MQ width is defined here by assuming that the nodes are of uniform distribution; the distance h in (35) is chosen as the equivalent grid size (i.e. $h = 1/(\sqrt{N} - 1)$). Figure 6 shows the solution accuracy N_e versus the grid size h for some constant values of β. Similar remarks to ODEs can be made here. It can be seen that highly accurate results are obtained. The relative L_2 error is reduced to $O(10^{-7})$ for $\beta = 4$. As β increases, the level of accuracy is clearly improved; however, their average rates are only about 3, e.g. 3.51 for $\beta = 1$, 3.45 for $\beta = 2$, 3.22 for $\beta = 3$, and 3.10 for $\beta = 4$, probably due to the use of unstructured nodes. In Figure 6, for large β, local rates/slopes are observed to vary with the grid size. Since global approximations result in full matrices, their computations can be very expensive. The global schemes are thus not suitable for large-scale applications. There is a need for having local schemes, which is discussed next.

4 IRBF Hermite-based method: local scheme

In a local version, only neighbouring nodes are activated for the approximation at a point. Consider a stencil associated with node i. For the Hermite type, some nodes on the stencil are selected to include information about ODE/PDE ($\mathcal{L}u = b$, $\mathcal{L}$ a linear differential operator, b a given function). Let n be the total number of nodes of the stencil and q the number of

special nodes just mentioned ($q < n$). A function is approximated as

$$u(\mathbf{x}) = \sum_{j=1}^{n} w_j \varphi(\|\mathbf{x} - \mathbf{x}_j\|) + \sum_{j=1}^{q} \bar{w}_j \mathcal{L}^{\bar{\mathbf{x}}_j} \varphi(\|\mathbf{x} - \bar{\mathbf{x}}_j\|) + \sum_{k=1}^{M} v_k p_k(\mathbf{x}), \tag{52}$$

where the notation $\mathcal{L}^{\bar{\mathbf{x}}_j}$ means that $\mathcal{L}$ acts on φ considered as a function of $\bar{\mathbf{x}}_j$, $\{\bar{\mathbf{x}}_j\}_{j=1}^{q}$ is a subset of $\{\mathbf{x}_j\}_{j=1}^{n}$, and $\{p_k(\mathbf{x})\}_{k=1}^{M}$ is a basis for the M-dimensional space ($\prod_m^d$) of all d-variate polynomials that have degree less than or equal to m. To account for the addition of polynomial terms, the following extra constraints are imposed

$$\sum_{j=1}^{n} w_j p_k(\mathbf{x}_j) + \sum_{j=1}^{q} \bar{w}_j \mathcal{L}^{\mathbf{x}} p_k(\mathbf{x})|_{\mathbf{x}=\bar{\mathbf{x}}_j} = 0, \quad k = 1, 2, \ldots, M. \tag{53}$$

Unlike Lagrange interpolation (function values only), expression (52) contains q extra coefficients (i.e. $\{\bar{w}_j\}_{j=1}^{q}$) that allow for the process of converting the RBF coefficient space into the physical space to take the form

$$\begin{pmatrix} u(\mathbf{x}_1) \\ \vdots \\ u(\mathbf{x}_n) \\ \mathcal{L}^{\mathbf{x}} u(\bar{\mathbf{x}}_1) \\ \vdots \\ \mathcal{L}^{\mathbf{x}} u(\bar{\mathbf{x}}_q) \\ 0 \\ \vdots \\ 0 \end{pmatrix} = \begin{bmatrix} \mathcal{C}^{11} & \mathcal{C}^{12} & \mathcal{C}^{13} \\ \mathcal{C}^{21} & \mathcal{C}^{22} & \mathcal{C}^{23} \\ \mathcal{C}^{31} & \mathcal{C}^{32} & \mathcal{C}^{33} \end{bmatrix} \begin{pmatrix} w_1 \\ \vdots \\ w_n \\ \bar{w}_1 \\ \vdots \\ \bar{w}_q \\ v_1 \\ \vdots \\ v_M \end{pmatrix}, \tag{54}$$

where the first n equations are for function values, the next q equations for derivative values (i.e. ODE/PDE), the last M equations for the extra constraints to account for the addition of polynomial terms, the square matrix on RHS is referred to as a conversion matrix, denoted

by $\mathcal{C}$, and

$$\left(\mathcal{C}^{11}\right)_{ij} = \varphi(\|\mathbf{x}_i - \mathbf{x}_j\|), \quad 1 \le i \le n,\ 1 \le j \le n, \tag{55}$$

$$\left(\mathcal{C}^{12}\right)_{ij} = \mathcal{L}^{\bar{\mathbf{x}}_j}\varphi(\|\mathbf{x}_i - \bar{\mathbf{x}}_j\|), \quad 1 \le i \le n,\ 1 \le j \le q, \tag{56}$$

$$\left(\mathcal{C}^{13}\right)_{ij} = p_j(\mathbf{x}_i), \quad 1 \le i \le n,\ 1 \le j \le M, \tag{57}$$

$$\left(\mathcal{C}^{21}\right)_{ij} = \mathcal{L}^{\mathbf{x}}\varphi(\|\mathbf{x} - \mathbf{x}_j\|)_{\mathbf{x}=\bar{\mathbf{x}}_i}, \quad 1 \le i \le q,\ 1 \le j \le n, \tag{58}$$

$$\left(\mathcal{C}^{22}\right)_{ij} = \mathcal{L}^{\mathbf{x}}\mathcal{L}^{\bar{\mathbf{x}}_j}\varphi(\|\mathbf{x} - \bar{\mathbf{x}}_j\|)_{\mathbf{x}=\bar{\mathbf{x}}_i}, \quad 1 \le i \le q,\ 1 \le j \le q, \tag{59}$$

$$\left(\mathcal{C}^{23}\right)_{ij} = \mathcal{L}^{\mathbf{x}}p_j(\mathbf{x})|_{\mathbf{x}=\bar{\mathbf{x}}_i}, \quad 1 \le i \le q,\ 1 \le j \le M, \tag{60}$$

$$\left(\mathcal{C}^{31}\right)_{ij} = p_i(\mathbf{x}_j), \quad 1 \le i \le M,\ 1 \le j \le n, \tag{61}$$

$$\left(\mathcal{C}^{32}\right)_{ij} = \mathcal{L}^{\mathbf{x}}p_i(\mathbf{x})|_{\mathbf{x}=\bar{\mathbf{x}}_j}, \quad 1 \le i \le M,\ 1 \le j \le q, \tag{62}$$

$$\left(\mathcal{C}^{33}\right)_{ij} = 0, \quad 1 \le i \le M,\ 1 \le j \le M. \tag{63}$$

When the RBF approximations are not augmented with the polynomial terms, the conversion system reduces to

$$\begin{pmatrix} u(\mathbf{x}_1) \\ \vdots \\ u(\mathbf{x}_n) \\ \mathcal{L}^{\mathbf{x}}u(\bar{\mathbf{x}}_1) \\ \vdots \\ \mathcal{L}^{\mathbf{x}}u(\bar{\mathbf{x}}_q) \end{pmatrix} = \begin{bmatrix} \mathcal{C}^{11} & \mathcal{C}^{12} \\ \mathcal{C}^{21} & \mathcal{C}^{22} \end{bmatrix} \begin{pmatrix} w_1 \\ \vdots \\ w_n \\ \bar{w}_1 \\ \vdots \\ \bar{w}_q \end{pmatrix}, \tag{64}$$

It can be seen that $\mathcal{C}$ is a symmetric matrix of dimensions $[n+q+M, n+q+M]$ if the polynomial terms are included and of dimensions $[n+q, n+q]$ if the polynomial terms are excluded. Making use of (54) and (64), a function and its derivatives at a point on the stencil can be expressed in terms of function values at $\{\mathbf{x}_j\}_{j=1}^{n}$, which are nodal unknowns to be found, and derivative values at $\{\bar{\mathbf{x}}_j\}_{j=1}^{q}$, which can be derived from the ODE/PDE.

By collocating the ODE/PDE at the interior grid nodes, and then replacing the obtained nodal derivative values with nodal variable values on their associated stencils, the ODE/PDE is transformed into a set of algebraic equations, which can be solved for the values of u at the grid nodes.

4.1 ODEs

We apply the methods to the following second-order ODE

$$d^2u/dx^2 = \exp(-40x)\left(1500\sin(10x) - 800\cos(10x)\right), \quad 0 \le x \le 1,$$

subject to Dirichlet boundary conditions. The exact solution can be verified to be $u_e(x) = \sin(10x)\exp(-40x)$. The domain is represented by sets of equi-spaced nodes. A stencil associated with node $\mathbf{x}_i$ is proposed to have 3 nodes. We take the distance h as the grid size. In contrast to the global approximation case, the value of β here can be chosen to be much larger.

Figure 7 shows the effects of β on the solution accuracy N_e. Results by the DRBF Hermite-based method are also included. For both methods, their systems are tri-diagonal and of the same dimensions. It can be seen that IRBF outperforms DRBF over a wide range of β. As β increases, the RBF approximations can be more accurate but its interpolation matrix condition number also grows quickly, making the computed error N_e fluctuating at large values of β. One can bypass this issue by using extended precision in computation. In [37], numerical investigations indicated that the condition number of the conversion matrix grows much faster than that of the final system matrix. Here, we only employ extended precision for constructing and inverting small conversion matrices (other computational parts including the solving of the final system of equations are conducted using double precision). The obtained results are also depicted in Figure 7. At low values of β, where the matrix is not ill-conditioned, double and extended precision basically yield the same errors. At large values of β, by extending the calculation precision, fluctuations in the computed error are eliminated.

Table 1 displays the computed solutions by several numerical methods. When compared to the classical central difference scheme, the compact approximations produce much more accurate results. Both compact FD [38] and IRBF methods are able to yield high rates of convergence (about fourth-order accuracy). To this problem, since its exact solution is available, the best values of β can be determined and their corresponding solutions are also

included in the table, which show that (i) the RBF accuracy can be further improved by varying β; and (ii) the simple formula (35) can work well for relatively-coarse grids.

4.2 PDEs

Like the global version, the present local methods are also meshless. However, our attention will be focused on the case of using Cartesian grid to represent the problem domain. The main reason for us to pursue this kind of discretisation lies in its economic pre-processing, easy implementation and its ability to also work with non-rectangular domains.

For 2D problems, a stencil associated with node $\mathbf{x}_i$ is proposed to have 9 nodes

$$\begin{bmatrix} \mathbf{x}_3 & \mathbf{x}_6 & \mathbf{x}_9 \\ \mathbf{x}_2 & \mathbf{x}_5 & \mathbf{x}_8 \\ \mathbf{x}_1 & \mathbf{x}_4 & \mathbf{x}_7 \end{bmatrix} \tag{65}$$

where the fifth node (i.e. $\mathbf{x}_5$) is a node i in a global numbering. Four nodes 2, 4, 6 and 8 (i.e. nodes nearer to the stencil centre) are selected to include the PDE information.

For a stencil associated with an interior node that is near an irregular boundary (e.g. curved boundary), it is proposed that the stencil consists of regular and irregular nodes (Figure 10). Regular nodes are simply the intersection points of the stencil grid lines, while irregular nodes are generated from the intersection of the boundary and the stencil grid lines. As a result, for boundary stencils, the number of nodes are typically greater than 9. The imposition of information about PDE is also implemented at side nodes on the horizontal and vertical grid lines (i.e. 4 nodes).

4.2.1 Poisson equation

A PDE to be employed is Poisson equation, where its driving function and Dirichlet boundary conditions are derived from the following solution $u_e(x, y) = e^{-6(x+y)} \cos(2\pi x) \sin(2\pi y)$. Both rectangular and non-rectangular domains are considered. For the latter, a quarter of a circle

is chosen (Figure 11).

The effects of the MQ width on the solution accuracy by the IRBF and DRBF Hermite-based methods are displayed in Figure 8 for rectangular domain and in Figure 12 for non-rectangular domain. It can be seen that the IRBF solutions are generally more accurate than DRBF ones over a wide range of β. At large values of β, as expected, there are some fluctuations in the computed error N_e. To make the calculation stable, we employ extended precision in forming the conversion matrix and computing its inverse. Since other computational parts are carried out with double precision, a full range of β is explored with a reasonable computational cost. With extended precision, as shown in the two figures, fluctuations no longer occur in the computed error at large values of β.

In Figure 9, results by the compact IRBF, central difference and compact finite difference [38] methods are displayed. Similar to second-order ODEs, the compact approximations for PDEs outperform those based on the central differences. The compact IRBF and FD methods yield high rates of convergence (about fourth-order accuracy). Exploiting the exact solution, the best values of β can be found. It can be seen that the use of a fixed β for relatively coarse grids can lead to results that are very close to the ones corresponding to the best values of β. For non-rectangular domains, the problem domain is simply embedded in a rectangle that is discretised using Cartesian grids of $7 \times 7, 9 \times 9, \cdots, 31 \times 31$. Table 2 displays the results obtained by the compact IRBF scheme. The solution converges as $O(h^{3.88})$ for $\beta = 16$, $O(h^{3.99})$ for $\beta = 18$ and $O(h^{4.09})$ for $\beta = 20$.

4.2.2 Convection-diffusion equation

We test the proposed local method with the following steady-state convection-diffusion equation and boundary conditions

$$\frac{\partial^2 u}{\partial x^2} + \frac{\partial^2 u}{\partial y^2} - P_e \frac{\partial u}{\partial x} = 0, \quad 0 \leq x, y \leq 1, \tag{66}$$

$$u(x,0) = u(x,1) = 0, \quad 0 \le x \le 1, \tag{67}$$

$$u(0,y) = \sin(\pi y),\ u(1,y) = 2\sin(\pi y), \quad 0 \le y \le 1, \tag{68}$$

where P_e is the Péclet number. The exact solution to this problem is given by

$$u_e(x,y) = \exp(P_e x/2)\sin(\pi y)\left[2\exp(-P_e/2)\sinh(\sigma x) + \sinh(\sigma(1-x))\right] / \sinh(\sigma), \tag{69}$$

where $\sigma = \sqrt{\pi^2 + P_e^2/4}$. As P_e increases, the boundary layer will be formed. Its gradient becomes very steep at large P_e values, presenting a great challenge for any numerical simulation. We simply employ uniform grids to represent the problem domain. It is observed that the optimal RBF width occurs earlier with respect to the RBF width when P_e increases from 10 to 100 (Figure 13). In contrast to problems whose solutions are smooth, the most accurate approximation for convection-dominated problems takes place at relatively-low values of the RBF width, where the RBF system is known to be stable. Note that all smooth curves depicted here are obtained with double-precision computations. By simply taking $\beta = \{10, 8, 6, 4\}$ for $P_e = \{10, 20, 40, 80\}$, respectively, a fast rate of convergence (i.e. about 4) is achieved (Figure 14). Figure 15 displays the present RBF solutions for several P_e values. It can be seen that they are all captured very well. At high P_e values, there are no oscillations in the solution near the boundary layer.

5 Concluding remarks

In this study, we have introduced integrated RBFs into the Hermite interpolation method for the numerical solution of ODEs/PDEs. Its main purpose is to yield a new strong (collocation) form of IRBF whose interpolation matrices are symmetric and non-singular. Several schemes based on global and local approximations for rectangular and non-rectangular domains are presented. The extended precision approach is utilised to extend the working range of the IRBF width for a given grid size; numerical examples show an improvement in accuracy achieved over conventional compact IRBF Hermite-based methods. The local version is a preferred option for the handling of large-scale problems as it possesses several attractive

features, including (i) sparse system matrix; (ii) fast convergence rate; and (iii) its ability to also work with large values of the RBF width with a relatively low computational cost. Highly accurate results are obtained using relatively coarse grids.

Appendix

The following equation is utilised to derive the limit of the fourth-order cross derivative of function φ as $r \to 0$

$$\nabla^4 \varphi = \nabla^2 \nabla^2 \varphi, \tag{70}$$

or

$$\frac{\partial^4 \varphi}{\partial x^4} + 2\frac{\partial^4 \varphi}{\partial x^2 \partial y^2} + \frac{\partial^4 \varphi}{\partial y^4} = \left(\frac{\partial^2}{\partial x^2} + \frac{\partial^2}{\partial y^2}\right)\left(\frac{\partial^2 \varphi}{\partial x^2} + \frac{\partial^2 \varphi}{\partial y^2}\right). \tag{71}$$

Taking into account

$$\left(\frac{\partial r}{\partial x}\right)^2 + \left(\frac{\partial r}{\partial y}\right)^2 = 1, \quad \frac{\partial^2 r}{\partial x^2} + \frac{\partial^2 r}{\partial y^2} = \frac{1}{r}, \tag{72}$$

the RHS of (71) can be rewritten in terms of derivatives of φ with respect to r only, and the equation becomes

$$\frac{\partial^4 \varphi}{\partial x^4} + 2\frac{\partial^4 \varphi}{\partial x^2 \partial y^2} + \frac{\partial^4 \varphi}{\partial y^4} = \frac{d^4 \varphi}{dr^4} + \frac{2}{r}\frac{d^3 \varphi}{dr^3} - \frac{1}{r^2}\frac{d^2 \varphi}{dr^2} + \frac{1}{r^3}\frac{d\varphi}{dr}, \tag{73}$$

from there, as $r \to 0$, one can acquire

$$\frac{\partial^4 \varphi}{\partial x^2 \partial y^2} \to -\frac{1}{a^3} \quad \text{for DRBF},$$
$$\frac{\partial^4 \varphi}{\partial x^2 \partial y^2} \to \frac{a}{3} \quad \text{for IRBF}.$$

References

1. C.A. Micchelli, Interpolation of scattered data: distance matrices and conditionally positive definite functions, Constructive Approximation 2, (1986), 11-22.

2. W.R. Madych, Miscellaneous error bounds for multiquadric and related interpolators, Computers and Mathematics with Applications 24(12), (1992), 121-138.

3. E.J. Kansa, Multiquadrics - A scattered data approximation scheme with applications to computational fluid-dynamics - II. Solutions to parabolic, hyperbolic and elliptic partial differential equations, Computers and Mathematics with Applications 19(8/9), (1990), 147-161.

4. E.J. Kansa, H. Power, G.E. Fasshauer and L. Ling, A volumetric integral radial basis function method for time-dependent partial differential equations: I. Formulation, Engineering Analysis with Boundary Elements 28, (2004), 1191-1206.

5. N. Mai-Duy and R.I. Tanner, Computing non-Newtonian fluid flow with radial basis function networks, Int. J. Numer. Meth. Fluids 48, (2005), 1309-1336.

6. B. Sarler, A radial basis function collocation approach in computational fluid dynamics, CMES: Computer Modeling in Engineering & Sciences 7(2), (2005), 185-194.

7. M. Li, T. Jiang and Y.C. Hon, A meshless method based on RBFs method for nonhomogeneous backward heat conduction problem, Engineering Analysis with Boundary Elements 34(9), (2010), 785-792.

8. C.-M. Fan, C.-S. Chien, H.-F. Chan and C.-L. Chiu, The local RBF collocation method for solving the double-diffusive natural convection in fluid-saturated porous media, International Journal of Heat and Mass Transfer 57(2), (2013), 500-503.

9. M. Li, W. Chen and C.S. Chen, The localized RBFs collocation methods for solving high dimensional PDEs, Engineering Analysis with Boundary Elements 37(10), (2013), 1300-1304.

10. D. Stevens, H. Power and K.A. Cliffe, A solution to linear elasticity using locally supported RBF collocation in a generalised finite-difference mode, Engineering Analysis with Boundary Elements 37(1), (2013), 32-41.

11. F.J. Mohammed, D. Ngo-Cong, D.V. Strunin, N. Mai-Duy and T. Tran-Cong, Modelling dispersion in laminar and turbulent flows in an open channel based on centre manifolds using 1D-IRBFN method, Applied Mathematical Modelling, 38(14), (2014), 3672-3691.

12. M. Dehghan and V. Mohammadi, The numerical solution of FokkerPlanck equation with radial basis functions (RBFs) based on the meshless technique of Kansa's approach and Galerkin method, Engineering Analysis with Boundary Elements 47, (2014), 38-63.

13. A. Vidal, A.J. Kassab and E.A. Divo, A direct velocity-pressure coupling Meshless algorithm for incompressible fluid flow simulations, Engineering Analysis with Boundary Elements 72, (2016), 1-10.

14. H. Zheng, C. Zhang, Y. Wang, J. Sladek and V. Sladek, A meshfree local RBF collocation method for anti-plane transverse elastic wave propagation analysis in 2D phononic crystals, Journal of Computational Physics 305, (2016), 997-1014.

15. B. Fornberg and G. Wright, Stable computation of multiquadric interpolants for all values of the shape parameter, Computers and Mathematics with Applications 48(5-6), (2004), 853-867.

16. G.B. Wright and B. Fornberg, Scattered node compact finite difference-type formulas generated from radial basis functions, Journal of Computational Physics 212(1), (2006), 99-123.

17. C.-S. Huang, C.-F. Lee and A.H.-D. Cheng, Error estimate, optimal shape factor, and high precision computation of multiquadric collocation method, Engineering Analysis with Boundary Elements 31(7), (2007), 614-623.

18. C.-S. Huang, H.-D. Yen and A.H.-D. Cheng, On the increasingly flat radial basis function and optimal shape parameter for the solution of elliptic PDEs, Engineering Analysis with Boundary Elements 34(9), (2010), 802-809.

19. B. Fornberg, E. Larsson and N. Flyer, Stable computations with Gaussian radial basis functions, SIAM Journal on Scientific Computing 33(2), (2011), 869-892.

20. J. Rashidinia, G.E. Fasshauer and M. Khasi, A stable method for the evaluation of Gaussian radial basis function solutions of interpolation and collocation problems, Computers and Mathematics with Applications 72(1), (2016), 178-193.

21. N. Flyer, B. Fornberg, V. Bayona and G.A. Barnett, On the role of polynomials in RBF-FD approximations: I. Interpolation and accuracy, Journal of Computational Physics 321, (2016), 21-38.

22. Y.C. Hon and R. Schaback, On unsymmetric collocation by radial basis functions, Applied Mathematics and Computation 119(23), (2001), 177-186.

23. R.L. Hardy, Research results in the application of multiquadric equations to surveying and mapping problems, Survg Mapp. 35, (1975), 321332.

24. Z. Wu, Hermite-Birkhoff interpolation of scattered data by radial basis functions, Approximation Theory and its Applications 8(2), (1992), 1-10.

25. X. Sun, Scattered Hermite interpolation using radial basis functions, Linear Algebra and its Applications 207, (1994), 135-146.

26. G.E. Fasshauer, "Solving partial differential equations by collocation with radial basis functions," in Surface Fitting and Multiresolution Methods, A. LeMhaut, C. Rabut and L.L. Schumaker (Editors), Vanderbilt University Press, Nashville, 1997, p. 131-138.

27. H. Power and V. Barraco, A comparison analysis between unsymmetric and symmetric radial basis function collocation methods for the numerical solution of partial differential equations, Computers and Mathematics with Applications 43, (2002), 551-583.

28. E. Larsson and B. Fornberg, A numerical study of some radial basis function based solution methods for elliptic PDEs, Computers and Mathematics with Applications 46, (2003), 891-902.

29. A.I. Tolstykh and D.A. Shirobokov, Using radial basis functions in a "finite difference mode", CMES: Computer Modeling in Engineering & Sciences 7(2), (2005), 207-222.

30. N. Mai-Duy and T. Tran-Cong, Compact local integrated-RBF approximations for second-order elliptic differential problems, Journal of Computational Physics 230(12), (2011), 4772-4794.

31. N. Mai-Duy and T. Tran-Cong, Numerical solution of differential equations using multiquadric radial basis function networks, Neural Networks 14(2), (2001), 185-199.

32. L. Ling and M.R. Trummer, Multiquadric collocation method with integral formulation for boundary layer problems, Computers and Mathematics with Applications 48(5-6), (2004), 927-941.

33. S.A. Sarra, Integrated multiquadric radial basis function approximation methods, Computers and Mathematics with Applications 51(8), (2006), 1283-1296.

34. C. Shu and Y.L. Wu, Integrated radial basis functions-based differential quadrature method and its performance, International Journal for Numerical Methods in Fluids 53(6), (2007), 969-984.

35. C.S. Chen, C.M. Fan and P.H. Wen, The method of approximated particular solutions for solving certain partial differential equations, Numerical Methods for Partial Differential Equations 28(2), (2010), 506-522.

36. N. Mai-Duy and T. Tran-Cong, A compact five-point stencil based on integrated RBFs for 2D second-order differential problems, Journal of Computational Physics 235, (2013), 302-321.

37. N. Mai-Duy, T.T.V. Le, C.M.T. Tien, D. Ngo-Cong and T. Tran-Cong, Compact approximation stencils based on integrated flat radial basis functions, Engineering Analysis with Boundary Elements 74, (2017), 79-87.

38. L. Collatz, The Numerical Treatment of Differential Equations, Springer-Verlag, Berlin, 1966.

Table 1: ODE, double precision: Relative L_2 errors of the computed solutions. Compact approximations outperform those based on the classical central differences. Both compact FD and IRBF schemes are able to yield high rates of convergence with respect to grid refinement. Given an analytic form of the solution u, the best values of β can be determined numerically and their corresponding solutions are also included for comparison purposes.

$N_x \times Ny$	FDM	Compact FDM	Compact IRBF, $\beta = 20$	Compact IRBF, optimal β
31×31	1.9807e+00	3.4981e-01	3.4935e-01	3.2995e-01
51×51	7.4623e-01	4.5186e-02	4.5034e-02	4.0292e-02
71×71	3.8853e-01	1.1845e-02	1.1760e-02	1.0211e-02
91×91	2.3735e-01	4.3536e-03	4.3270e-03	3.6870e-03
111×111	1.5973e-01	1.9559e-03	1.9408e-03	1.6401e-03
131×131	1.1473e-01	1.0043e-03	9.9094e-04	8.3703e-04
151×151	8.6348e-02	5.6717e-04	5.4784e-04	4.7088e-04
171×171	6.7319e-02	3.4403e-04	3.2732e-04	2.8486e-04
191×191	5.3945e-02	2.2060e-04	2.1582e-04	1.8228e-04
211×211	4.4191e-02	1.4788e-04	1.3573e-04	1.2193e-04
	$O(h^{1.96})$	$O(h^{3.99})$	$O(h^{4.02})$	$O(h^{4.07})$

Table 2: PDE, non-rectangular domain, double precision: Grid convergence by the local IRBF Hermite-based scheme for several RBF widths .

	Relative L_2 error		
$N_x \times Ny$	$\beta = 16$	$\beta = 18$	$\beta = 20$
7×7	1.8576e-02	1.8407e-02	1.8324e-02
9×9	4.0162e-03	3.9526e-03	3.9217e-03
11×11	1.4255e-03	1.3987e-03	1.3714e-03
13×13	6.5265e-04	6.2664e-04	6.1840e-04
15×15	3.5023e-04	3.3471e-04	3.2295e-04
17×17	2.1138e-04	1.9490e-04	1.8655e-04
19×19	1.3937e-04	1.2728e-04	1.2112e-04
21×21	9.8276e-05	8.8445e-05	8.0223e-05
23×23	7.3275e-05	6.2924e-05	5.8075e-05
25×25	5.6198e-05	4.8013e-05	4.4473e-05
27×27	4.4900e-05	3.8746e-05	3.7525e-05
29×29	3.6775e-05	3.1344e-05	2.4388e-05
31×31	3.0377e-05	2.6381e-05	2.2324e-05
	$O(h^{3.88})$	$O(h^{3.99})$	$O(h^{4.09})$

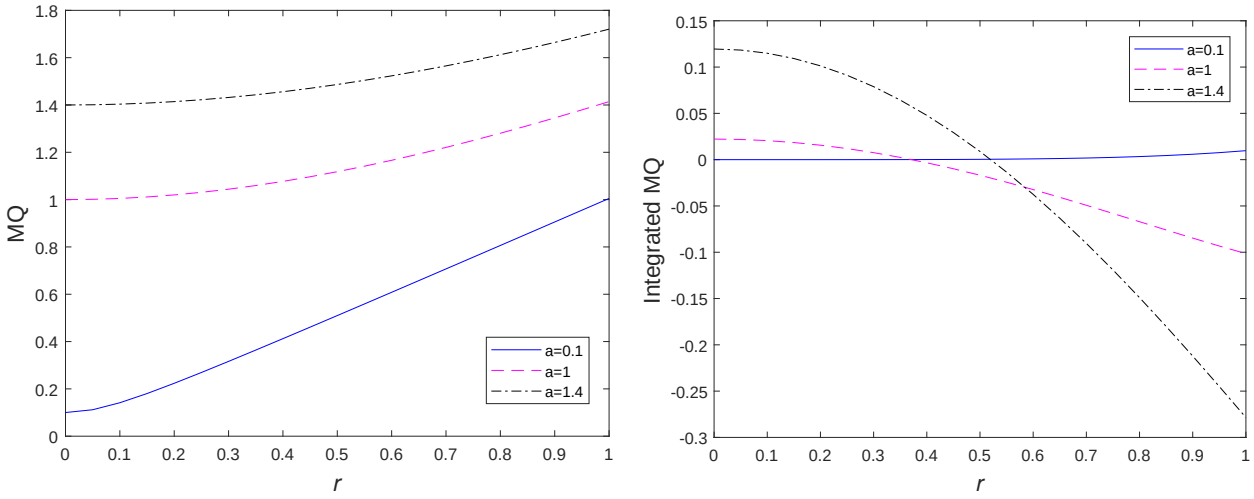

Figure 1: Variations of the MQ (left) and integrated MQ (right) for several values of the MQ width a.

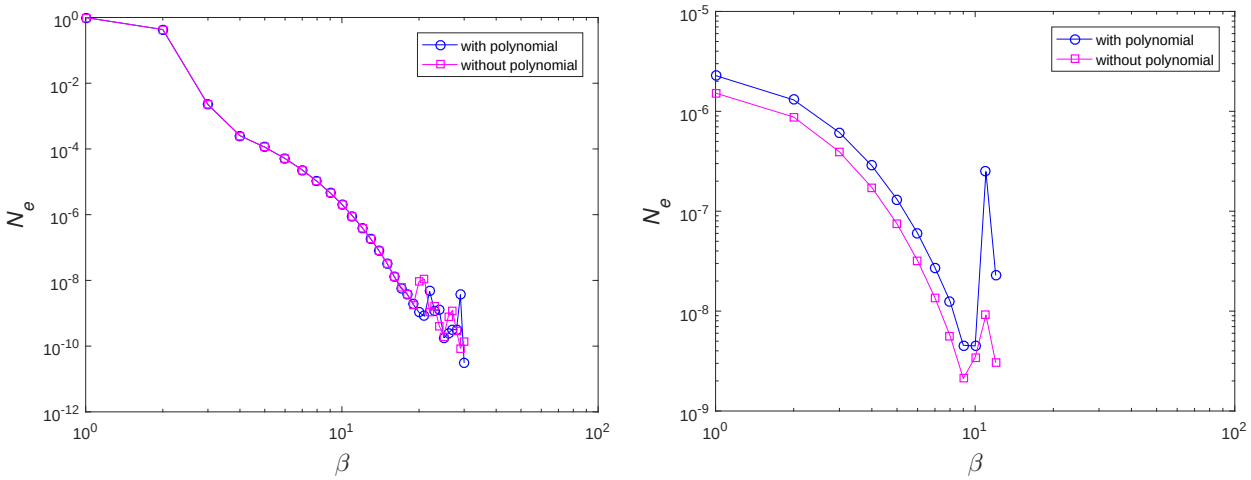

Figure 2: Second-order ODE, 151 grid nodes: Effects of the augmented polynomial in the RBF approximations on their solution accuracy over a wide range of the RBF width by the global DRBF (left) and IRBF (right) Hermite-based methods

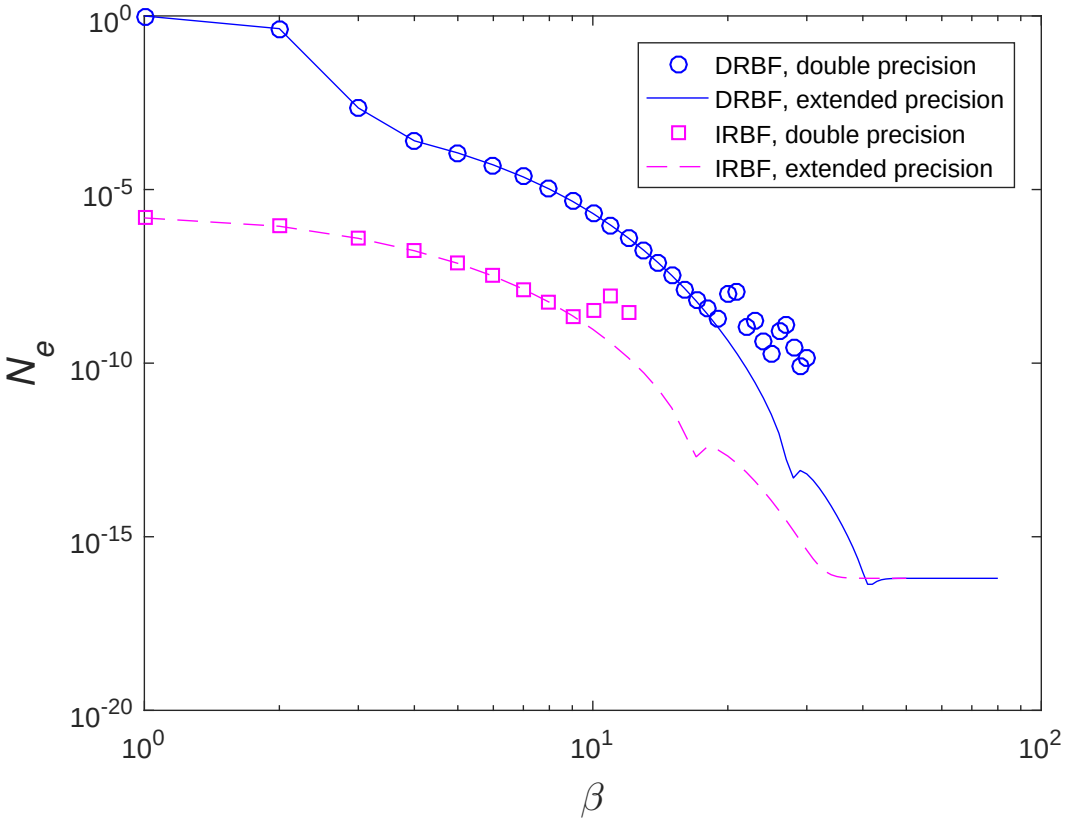

Figure 3: Second-order ODE, 151 grid nodes, double/extended precision: Effects of the RBF width on the solution accuracy by the global Hermite-based methods.

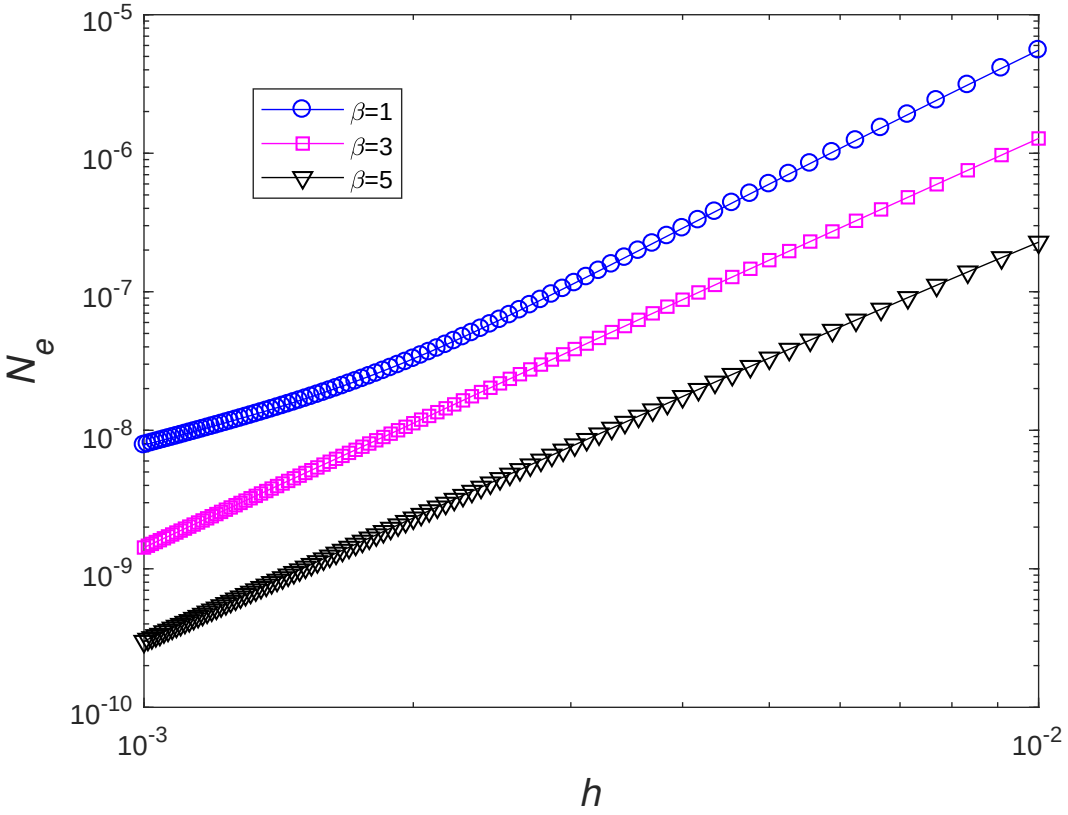

Figure 4: Second-order ODE, double precision: Grid convergence by the proposed global Hermite-based method for several values of β.

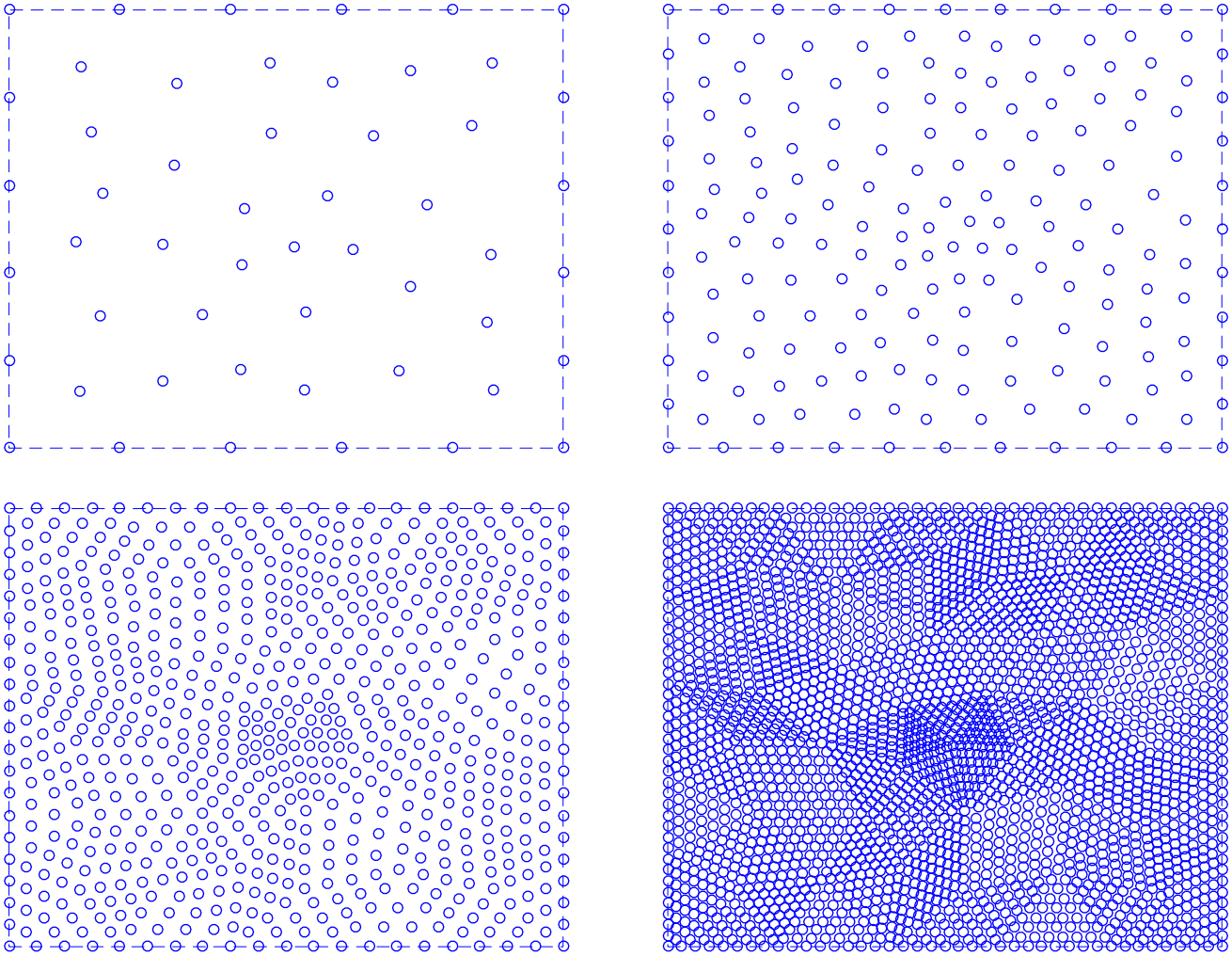

Figure 5: Domain discretisations using 52, 185, 697 and 2705 unstructured nodes.

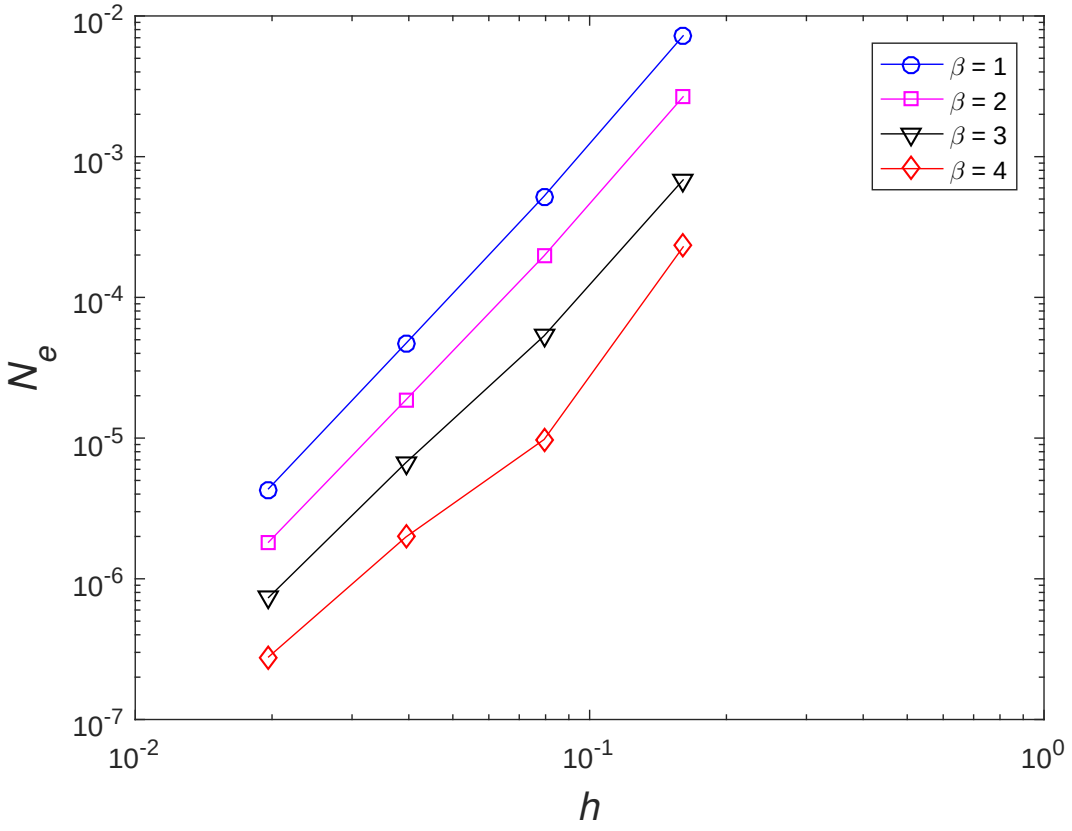

Figure 6: PDE, double precision: Grid convergence by the proposed global Hermite-based method for several values of β.

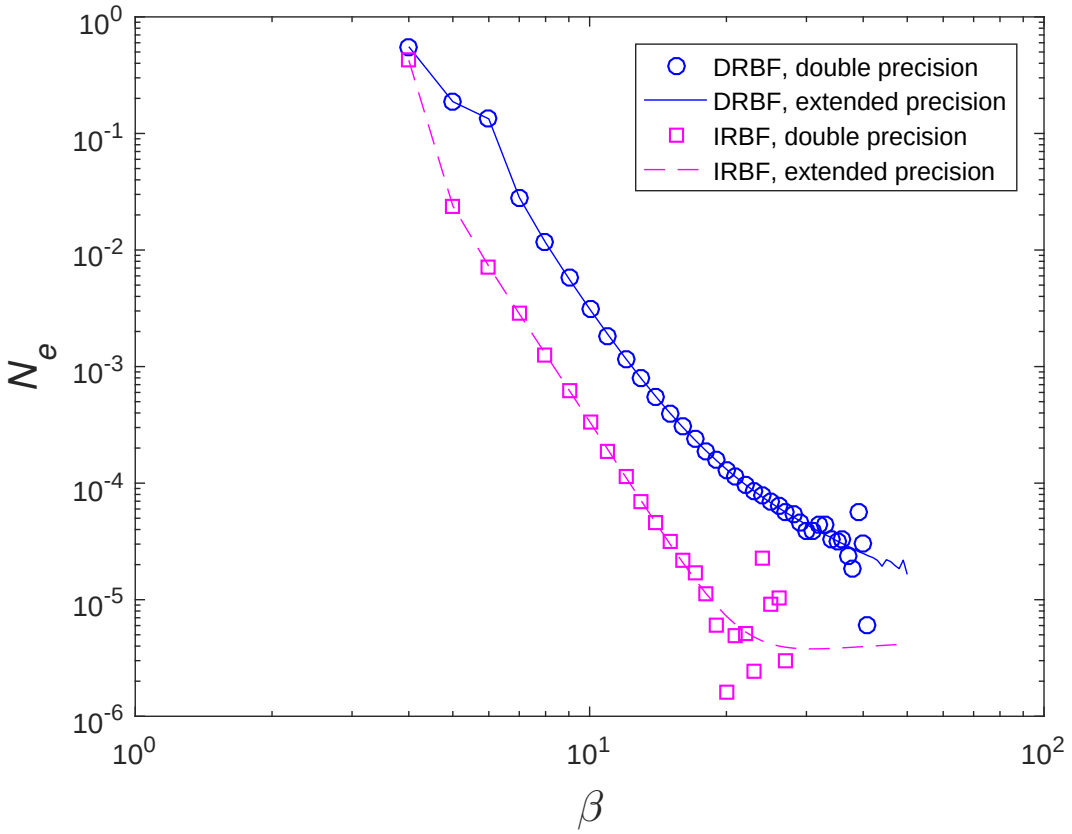

Figure 7: Second-order ODE, $N = 501$, double/extended precision: Effects of the RBF width (represented through β) on the solution accuracy by the local Hermite-based methods. Both DRBF and IRBF schemes are examined over a wide range of β.

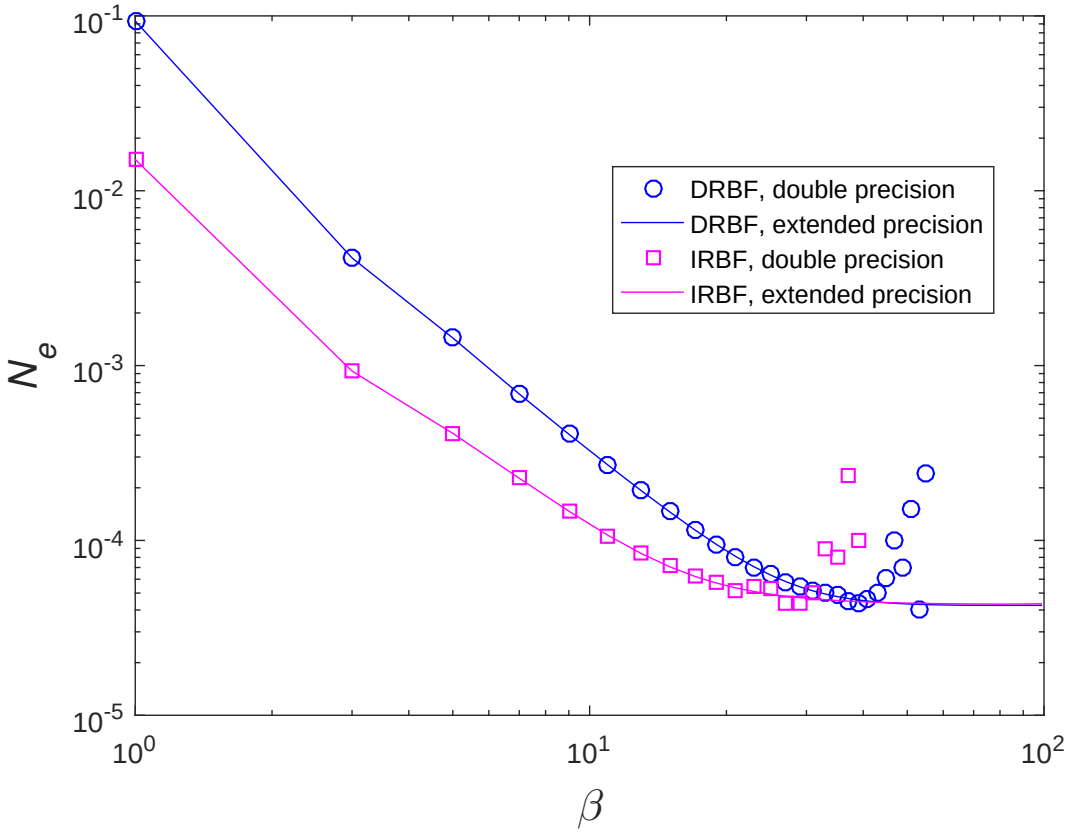

Figure 8: Poisson equation, rectangular domain, 21×21, double/extended precision: Effects of the RBF width (represented through β) on the solution accuracy by the local Hermite-based methods. Both DRBF and IRBF schemes are examined over a wide range of β.

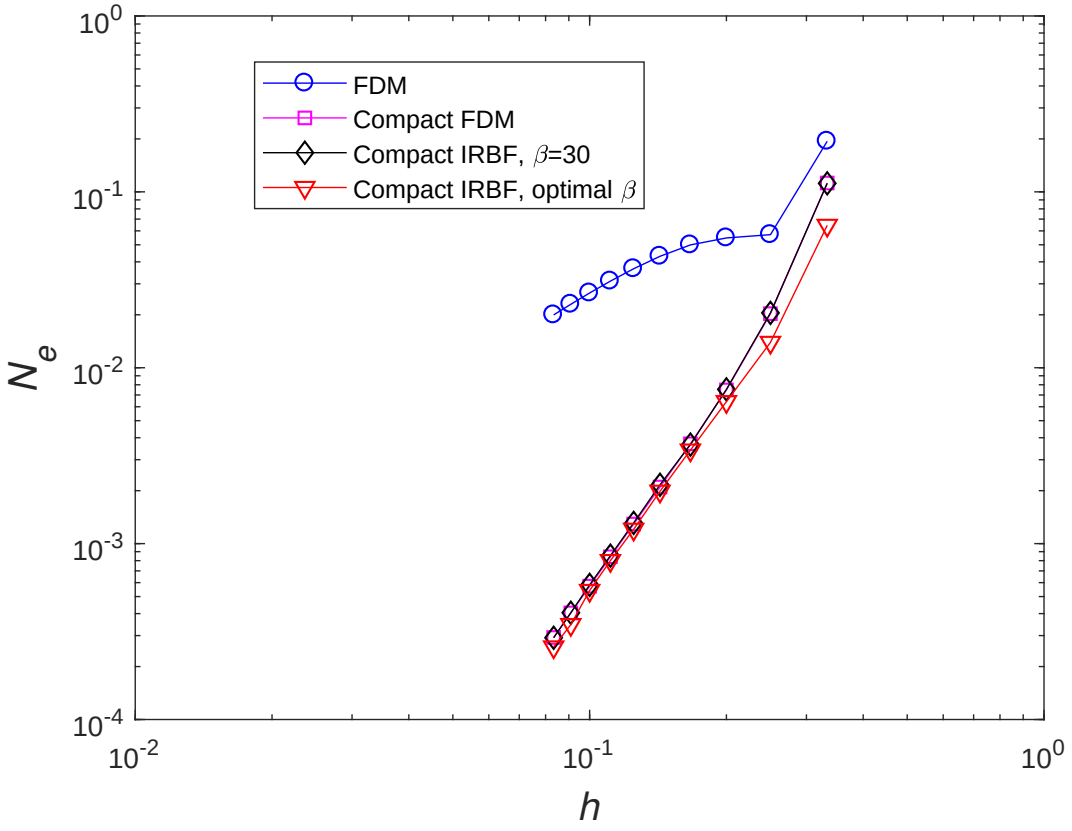

Figure 9: Poisson equation, rectangular domain, $\beta = 30$, double precision: Comparison of accuracy between the compact IRBF scheme and FDMs (central difference (CD) and compact). The computed solution converges apparently as $O(h^{1.34})$, $O(h^{4.11})$ and $O(h^{4.11})$ for the CD, compact FD and compact IRBF methods, respectively. The IRBF results at the best values of β are also included for comparison purposes.

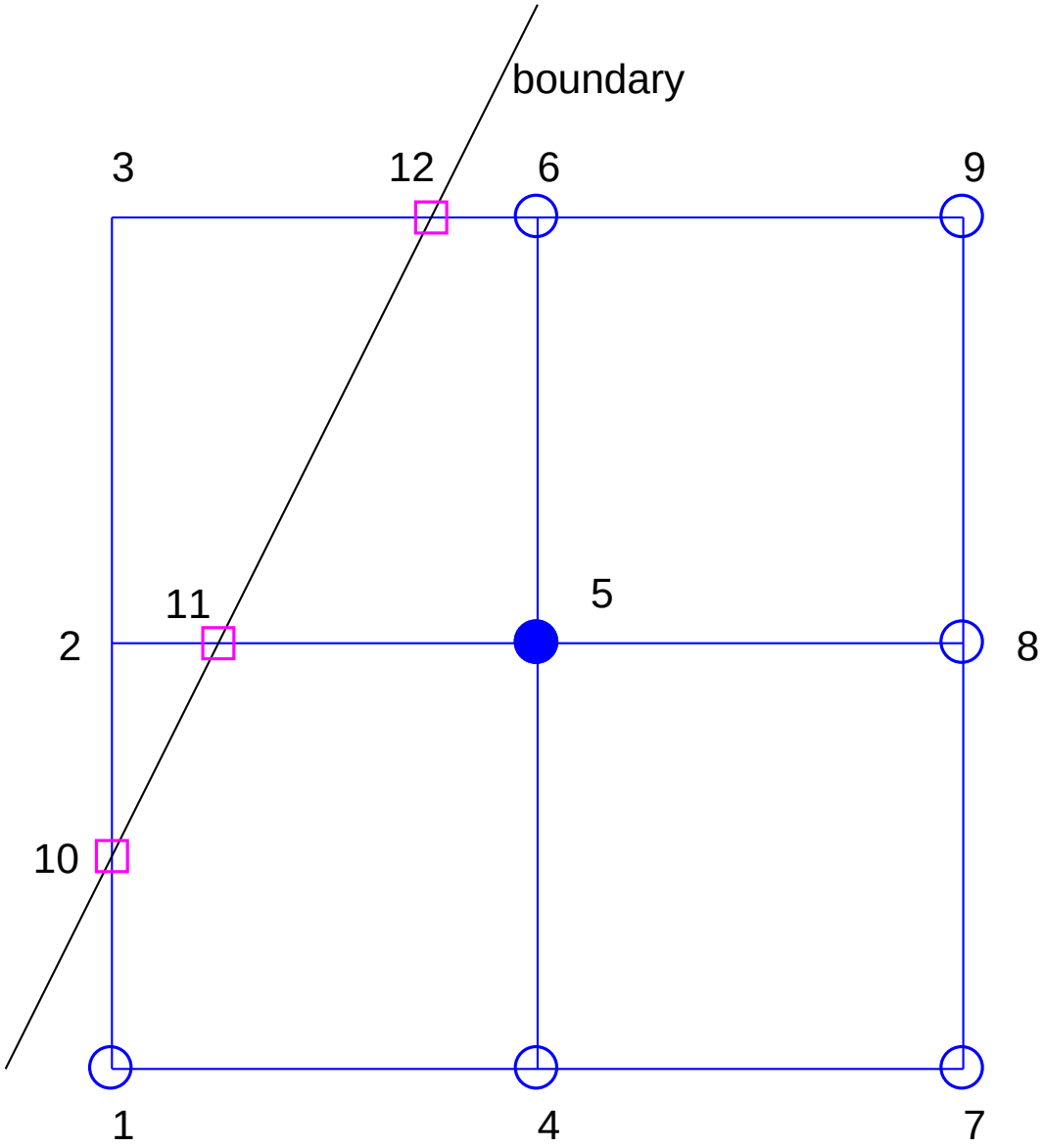

Figure 10: Non-rectangular domain: a schematic diagram for boundary stencils. The stencil, which is associated with node 5, consists of regular nodes: (1,4,5,6,7,8,9) and irregular nodes: (10,11,12). The PDE is imposed at side nodes: (11,4,6,8).

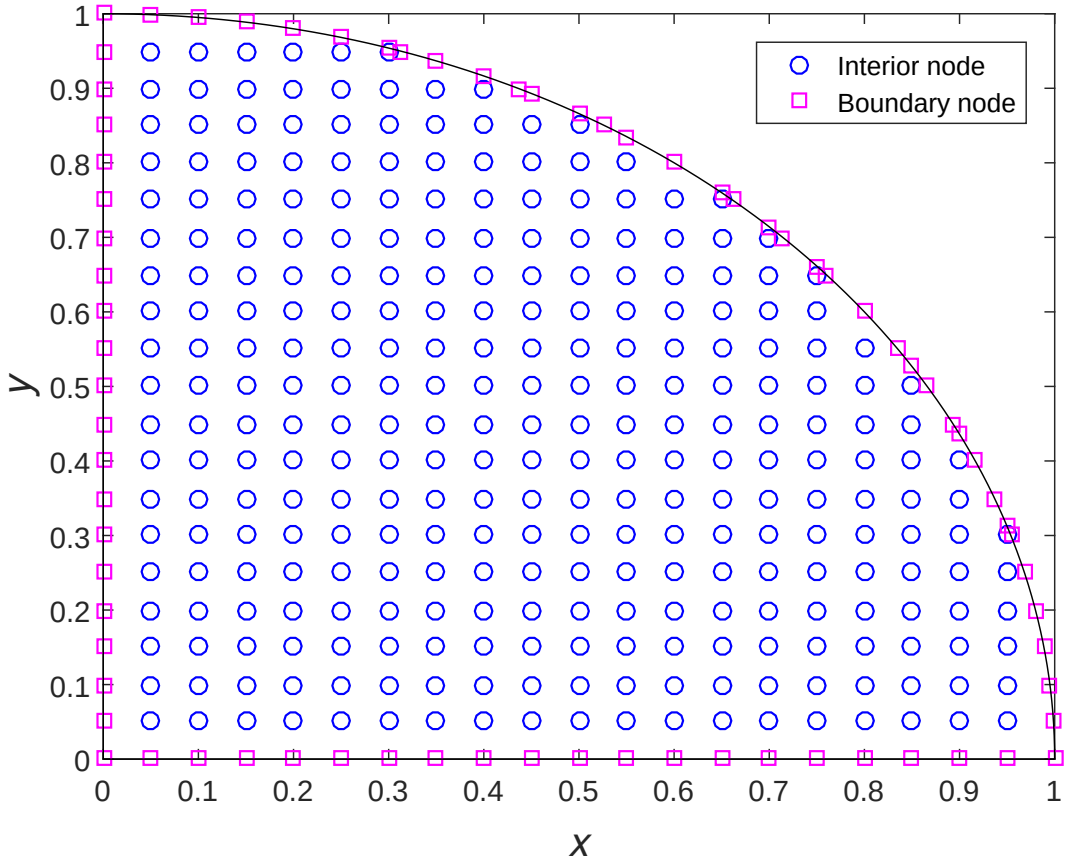

Figure 11: Non-rectangular domain: The problem domain is embedded in a rectangle that is then discretised by a Cartesian grid. Interior nodes are grid nodes within the problem domain. Boundary nodes are generated by the intersection of the grid lines and the boundary of the domain.

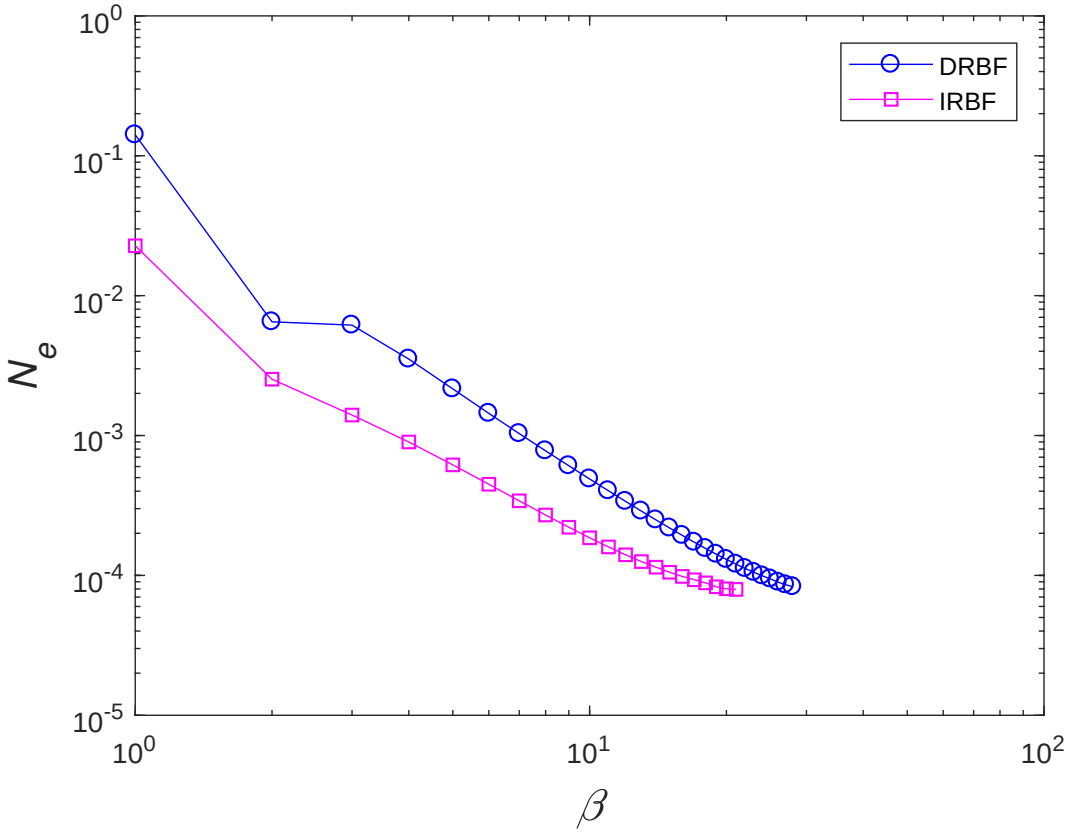

Figure 12: Poisson equation, nonrectangular domain, double precision: Effects of the RBF width on the solution accuracy by the local Hermite-based methods.

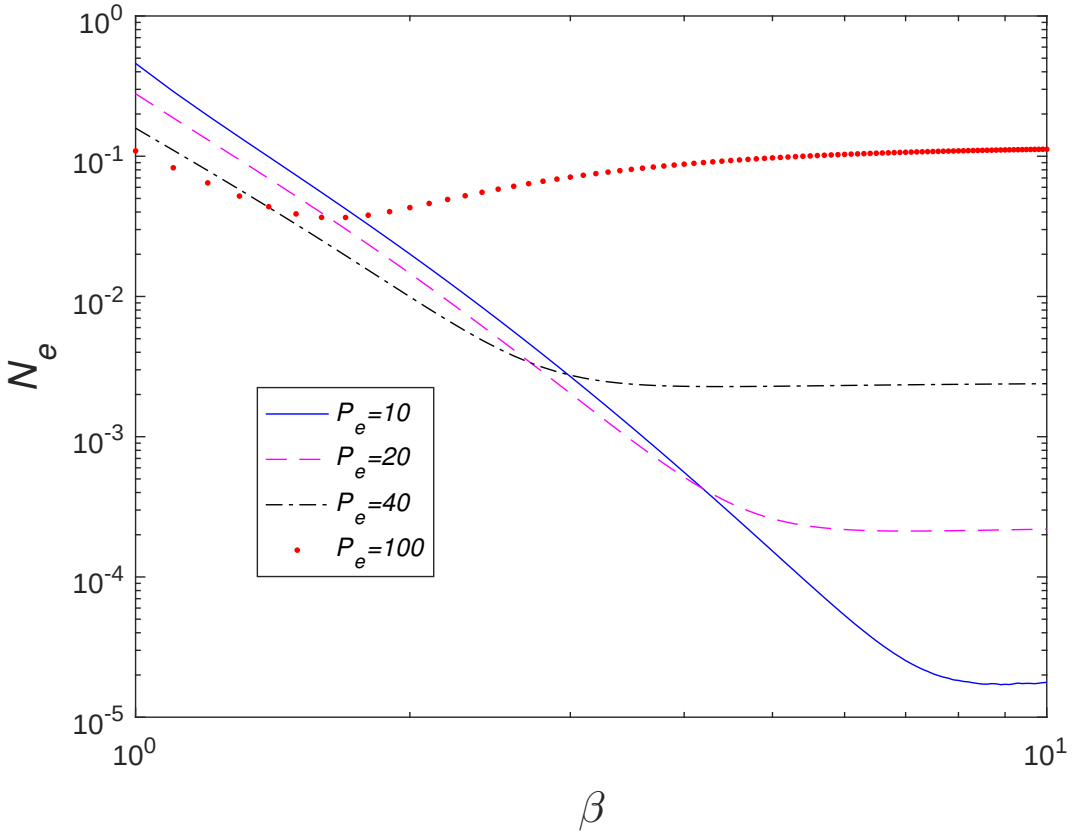

Figure 13: Convection-diffusion equation, 33×33, double precision: Effects of the RBF width on the solution accuracy for several Péclet numbers by the proposed local Hermite-based method.

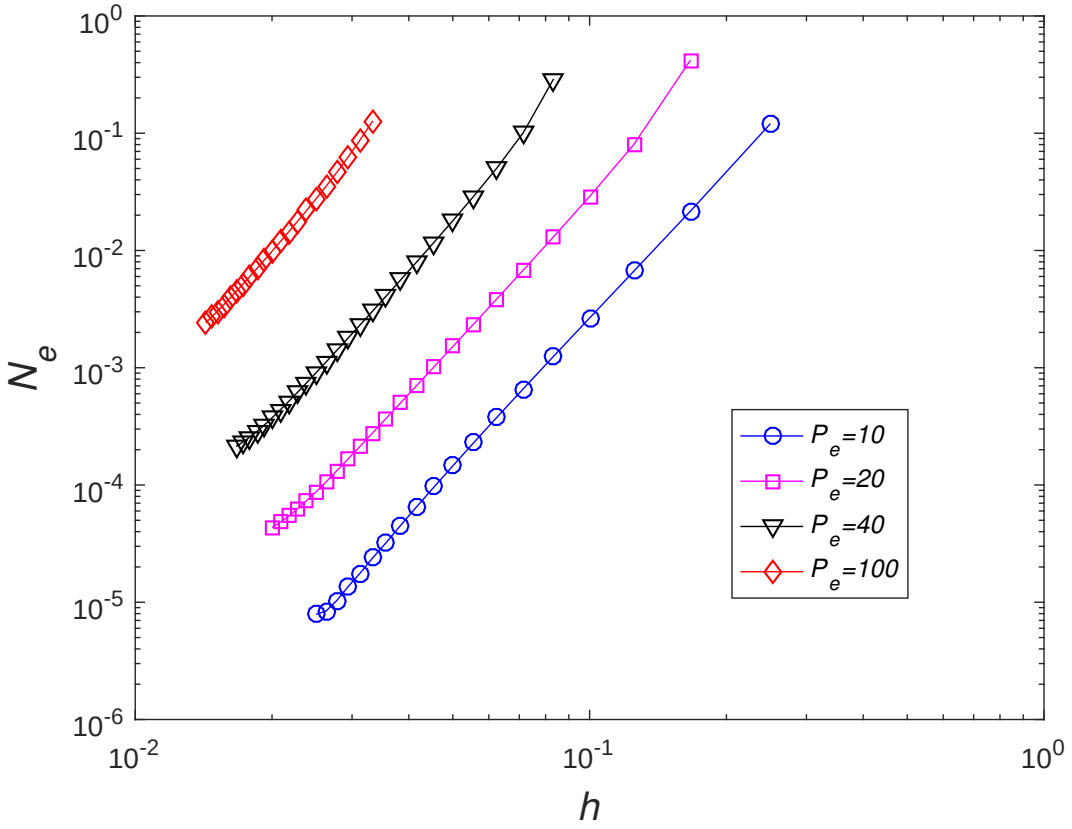

Figure 14: Convection-diffusion equation, double precision: Effects of the grid size on the solution accuracy for several Péclet numbers by the proposed local Hermite-based method. Values of β used are $\{10,\ 8,\ 6,\ 4\}$ for $P_e = \{10, 20, 40, 100\}$, respectively. The solution converges as $O(h^{4.24})$ for $P_e = 10$, $O(h^{4.23})$ for $P_e = 20$, $O(h^{4.34})$ for $P_e = 40$ and $O(h^{4.61})$ for $P_e = 100$.

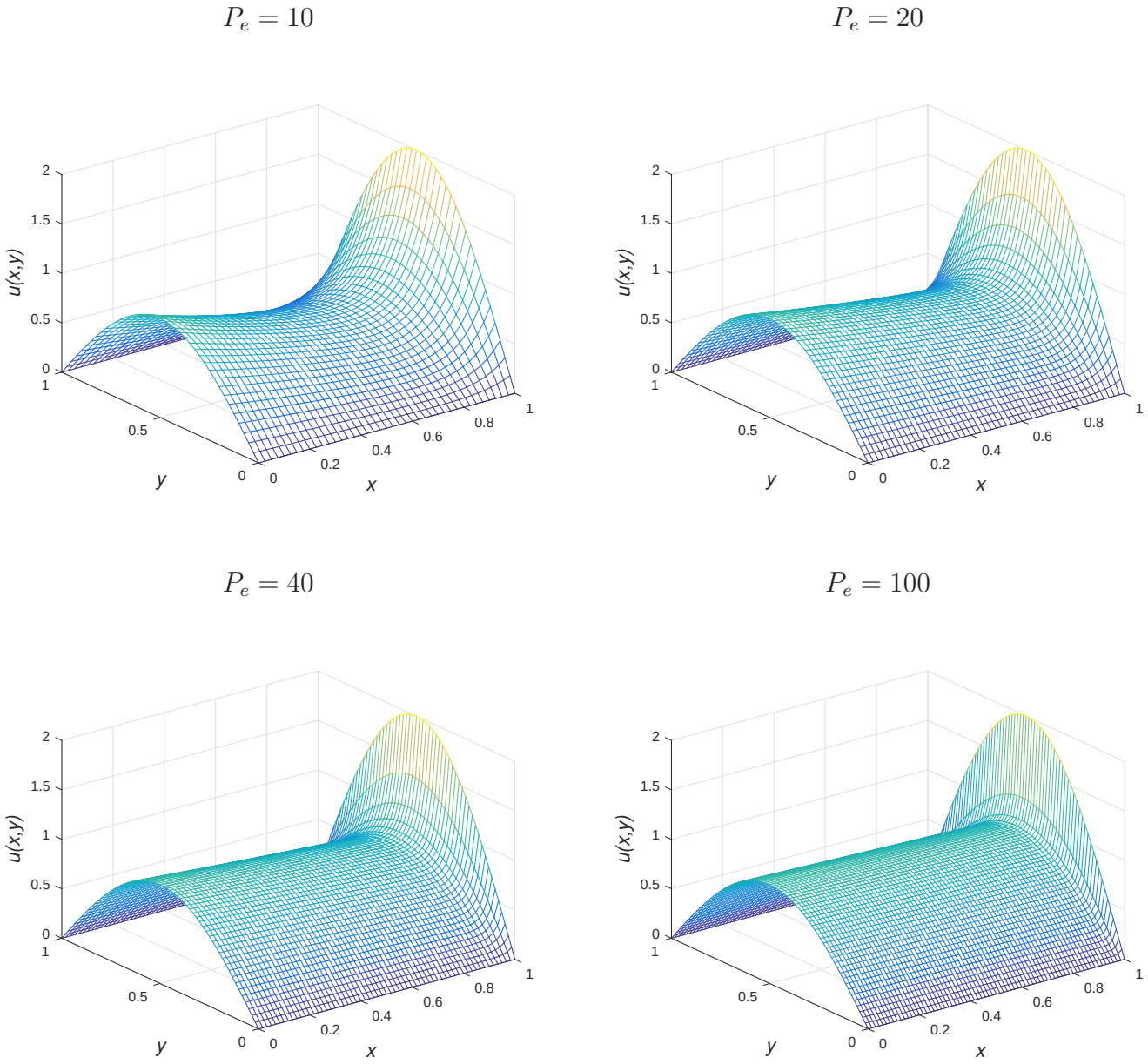

Figure 15: Convection-diffusion equation, double precision: Numerical solutions by the proposed local Hermite-based method using grid of 41×41 for $P_e = 10$, 51×51 for $P_e = 20$, 61×61 for $P_e = 40$ and 71×71 for $P_e = 100$.